

# Melting and Freezing of a Skyrmion Lattice

Dmitry A. Garanin, Jorge F. Soriano, and Eugene M. Chudnovsky

*Physics Department, Herbert H. Lehman College and Graduate School, The City University of New York,  
250 Bedford Park Boulevard West, Bronx, New York 10468-1589, USA*

(Dated: June 4, 2024)

We report comprehensive Monte-Carlo studies of the melting of skyrmion lattices in systems of small, medium, and large sizes with the number of skyrmions ranging from  $10^3$  to over  $10^5$ . Large systems exhibit hysteresis similar to that observed in real experiments on the melting of skyrmion lattices. For sufficiently small systems which achieve thermal equilibrium, a fully reversible sharp solid-liquid transition on temperature with no intermediate hexatic phase is observed. A similar behavior is found on changing the magnetic field that provides the control of pressure in the skyrmion lattice. We find that on heating the melting transition occurs via a formation of grains with different orientations of hexagonal axes. On cooling, the fluctuating grains coalesce into larger clusters until a uniform orientation of hexagonal axes is slowly established. The observed scenario is caused by collective effects involving defects and is more complex than a simple picture of a transition driven by the unbinding and annihilation of dislocation and disclination pairs.

## I. INTRODUCTION

Recently, several groups have reported theoretical and experimental studies of the melting of skyrmion lattices (SkL) in ferromagnetic films [1–8]. They have been driven by the interest to the fundamental problem of crystallinity and melting transition in two dimensions (2D), which generated controversies for almost a century of theoretical and experimental research, see, e.g., Refs. [9, 10] for review. This paper contains a detailed study of the melting of the skyrmion lattice. The brief history of the subject is outlined below.

The study of 2D crystals began with the work of Peierls [11] who had shown that in 2D the average square deviation of atoms ( $\mathbf{u}^2$ ) from equilibrium positions in a crystal diverges with the size of the system  $L$  as  $\ln L$  due to thermal fluctuations. Thirty years later, Mermin and Wagner [12], and independently Hohenberg, [13] argued that the long-range order cannot exist in 2D not only for crystals but also for magnets (no net magnetization) and superfluids (no Bose condensation). This, however, contradicted the numerical work on hard disks [14] performed in the early 1960s, which showed a melting transition between solid and liquid states. Also, contrary to the theory, the superfluidity in 2D helium films was demonstrated experimentally in the late 1960s [15]. It was subsequently realized that while fluctuations indeed grew in 2D as  $\ln L$ , they did not prevent the system from developing rigidity at low temperatures, which for a 2D crystal meant finite elastic moduli.

In 1971 Berezinskii demonstrated theoretically that the destruction of the long-range order in thin magnetic films and 2D crystals should occur through the creation of topological defects [16]. One year later, Kosterlitz and Thouless (KT) [17] arrived at the same conclusion for 2D solids and superfluids. The KT results for the temperature dependence of the superfluid density in a helium film were confirmed by Bishop and Reppy in the late 1970s [18]. Soon, however, Halperin and Nelson [19, 20], and independently Young [21], realized that as far as the

solids were concerned the KT theory was missing the angular terms in the energy of interaction between dislocations. By including such terms in the Hamiltonian, they showed that the melting of a 2D crystal occurred into an anisotropic liquid with the exponential decay of translational correlations but only the algebraic decay of orientational correlations, which they called a hexatic liquid. The latter, according to the KTHNY theory, melted into the isotropic liquid due to the creation of disclinations via a second transition at a higher temperature.

In contrast with the KTHNY theory, however, early simulations that used molecular dynamics, see, e.g., Ref. [22], emphasized the importance of short-wave phonons that can drive a conventional first-order melting in 2D as they do in 3D via the Lindemann melting criterion [23]. (It was recently suggested [24] that in 2D the Lindemann criterion essentially coincides with the KTHNY condition for spontaneous creation of dislocations). In addition, in the early 1980s, Chui [25] and independently Saito [26], considering the 2D melting problem in terms of interacting dislocations, argued that the KTHNY scenario of melting via the spontaneous creation of independent dislocation pairs by thermal agitation was self-consistent only at a sufficiently large energy of the dislocation core, compared to their interaction energy. As the core energy is lowered, dislocations are created in clusters. Close to the transition temperature they aggregate into the grain boundaries that break the 2D crystal into differently oriented grains. Such a possibility was first acknowledged in the earlier studies of the melting of a 2D electron crystal [27]. The energy of the dislocation core is difficult to measure directly and it requires a computation at the level of individual atoms. The lack of that knowledge creates the biggest uncertainty about the nature of the melting transition in a 2D system.

Numerous experimental studies performed on 2D crystals in the 1980s and 1990s, see e.g. Ref. [28], showed a first-order melting transition, as in 3D, with no sign of the hexatic phase. The existence of the latter at low temperatures due to disorder was predicted [29, 30] and observed

in vortex lattices of type-II superconductors [31], but convincing evidence of the thermally induced KTHNY two-step melting emerged from the study of lattices of colloidal particles [32, 33] only in the 2000s. Subsequently, it was established by numerous studies that the melting scenario was not universal. Besides the energy of the dislocation core, it depends on the interaction potential, the shape of the interacting particles, and the symmetry of the crystal lattice, see, e.g., Refs. [34–37] and references therein.

The interest in skyrmions in magnetic films, besides the beauty of the physics [38] and imagery associated with them, has been driven by the prospect of developing topologically protected information technology [39–43]. In materials lacking inversion symmetry, individual skyrmions are stabilized by Dzyaloshinskii-Moriya interaction (DMI) [44–49]. Other mechanisms of stabilization of skyrmions include frustrated exchange interactions [50, 51], magnetic anisotropy [52, 53], disorder [54], and geometrical confinement [55].

Theoretical research on 2D lattices of magnetic vortices in systems with Dzyaloshinskii-Moriya (DMI) interaction was pioneered by Bogdanov and Hubert [45]. They obtained the magnetic phase diagram separating the conventional laminar domain structure from the magnetic state with a periodic arrangement of vortices. The first evidence of regular skyrmion lattices was reported in FeCoSi films by Yu et al. [56] with the help of the real-space Lorentz transmission electron microscopy. It was followed by an avalanche of papers demonstrating transitions between uniformly magnetized states, laminar domains, and skyrmion crystals on the magnetic field and temperature, see, e.g., Refs. [57, 58] and references therein.

In recent years it was realized that the skyrmion lattice (see Fig. 1) provides another rich system for the study of 2D melting. An advantage here is that the melting transition can be achieved on both temperature and the magnetic field. Conflicting results have been obtained so far by theorists and experimentalists. Nishikawa et al. [2] used Monte Carlo simulations for the lattice-spins model to show a direct melting into an isotropic 2D liquid, with no evidence of the intermediate hexatic phase. Monte-Carlo studies [7] of lattices of up to  $10^5$  skyrmions considered as point particles with repulsive interaction obtained from a microscopic spin model [59] rendered a similar conclusion. However, measurements of Huang et al. [4] performed on a nano-slab of  $\text{Cu}_2\text{OSeO}_3$  by using cryo-Lorentz transmission electron microscopy reported a two-step KTHNY melting transition. Such a transition was also observed in the simulations of skyrmion lattices in a  $\text{GaV}_4\text{S}_8$  spinel by Baláz et al. [5].

Nonequilibrium effects hinder comparison with the analytical theory of the 2D melting that assumes thermal equilibrium. For example, thermal studies of skyrmion lattices in a stack of Ta(5)/Co<sub>20</sub>Fe<sub>60</sub>B<sub>20</sub>(0.9)/Ta(0.08)/MgO(2)/Ta(5) by Zavorka et al. [3], while providing good data on the

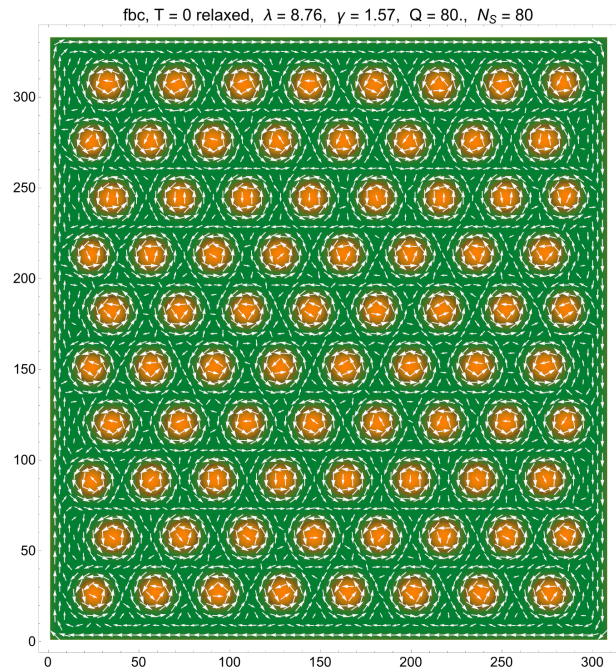


Figure 1. Triangular skyrmion lattice in the system with free boundary condition at  $T = 0$ . Spin components are color-coded,  $s_z = -1$  green,  $s_z = 1$  orange. White arrows show the in-plane spin components  $s_x$  and  $s_y$ .

orientational correlations, did not produce consistent results on the nature of the phase transition due to long equilibration times. McGray et al. [6] reported hysteresis in the temperature dependence of the orientational order in the skyrmion lattices of  $\text{Fe}_3\text{GeTe}_2$  similar to that in the field-cooled/zero-field-cooled (FC/ZFC) magnetization studies of the arrays of single-domain magnetic particles in a solid matrix [60]. According to Meisheimer et al. [8], disorder and pinning of skyrmions inhibited simple scenarios of the melting transition in a polar van der Waals magnet  $(\text{Fe}_{0.5}\text{Co}_{0.5})_5\text{GeTe}_2$ .

Such a broad range of melting scenarios in the skyrmion lattices can be explained by several factors. One factor can be the difference in the dislocation core energy for different materials. The slow equilibration in both experiments and numerical work is another factor. We try to overcome the latter problem in our Monte Carlo simulations while also elucidating nonequilibrium effects that can be seen in real experiments. Ambrose and Stamps [1] mentioned the distortion of the skyrmion profile on approaching the melting transition, which they observed in the Monte Carlo studies that used parameters of FeCoSi and FeGe. It was confirmed that such effect does exist at the melting transition where it is responsible for the kink in the temperature dependence of the magnetization [64]. Since the number of magnetic systems in which skyrmion lattices have been observed experimentally increases rapidly, in our studies we stuck to the most common range of parameters without specifying a concrete material. The goal is to elucidate features

of the skyrmion matter that may be seen in the melting and freezing of other 2D systems.

Apart from elucidating the thermodynamics of the melting/freezing transition, we investigate dislocations which spontaneously emerge when a 2D skyrmion solid is heated. The picture that we observe in Monte Carlo simulations and illustrate with images in the paper and with movies in the supplemental material, clearly points toward the Chui-Saito melting scenario [25, 26] in which the dislocations emerge in clusters on approaching the melting transition. At the transition, they aggregate into grain boundaries that break the 2D solid with a quasi-long-range orientational order into a system of fluctuating differently oriented grains. The transition is well defined by the abrupt change in the orientational order parameter. However, the orientationally ordered grains of fluctuating shape and size are also seen in the liquid phase. We study their properties with an eye on real experiments that can image the structure of the skyrmion matter near the melting/freezing transition.

The paper is organized as follows. The model of the skyrmion lattice, the order parameter, and the relevant thermodynamics are explained in Sec. II. The numerical method is described in Sec. III. Thermodynamic quantities, including the vicinity of the melting/freezing transition, are computed in Sec. IV. The characteristics of the defects that spontaneously emerge on rising temperature are computed and illustrated by images in Sec. V. The nonequilibrium effects are studied in Sec. VI. Our conclusions and suggestions for experiments are presented in Sec. VII.

## II. THE MODEL

### A. Skyrmions in the lattice-spins model

We consider skyrmions in the model of ferromagnetically coupled three-component classical spin vectors  $\mathbf{s}_i$  of length 1 on a square lattice with the energy given by

$$\mathcal{H} = -\frac{1}{2} \sum_{ij} J_{ij} \mathbf{s}_i \cdot \mathbf{s}_j - H \sum_i s_{iz} - A \sum_i [(\mathbf{s}_i \times \mathbf{s}_{i+\delta_x})_x + (\mathbf{s}_i \times \mathbf{s}_{i+\delta_y})_y]. \quad (1)$$

The nearest neighbors exchange interaction of strength  $J > 0$  favors ferromagnetic ordering and incorporates the actual length of the spin. The stabilizing field  $H$  in the second (Zeeman) term is applied in the negative  $z$ -direction,  $H < 0$ . The third term in Eq. (1) is the Dzyaloshinskii-Moriya interaction (DMI) of the Bloch type of strength  $A$ , with  $\delta_x$  and  $\delta_y$  standing for to the nearest lattice site in the positive  $x$  or  $y$  direction. In this configuration, the dominant direction of spins is down and that in the skyrmions is up. The DMI of the Néel type is described by the term  $(\mathbf{s}_i \times \mathbf{s}_{i+\delta_x})_y - (\mathbf{s}_i \times \mathbf{s}_{i+\delta_y})_x$  and leads to similar results.

Two-dimensional configurations of the spin field are characterized by the topological charge [38]

$$Q = \int \frac{dxdy}{4\pi} \mathbf{s} \cdot \frac{\partial \mathbf{s}}{\partial x} \times \frac{\partial \mathbf{s}}{\partial y} \quad (2)$$

that takes quantized values  $Q = 0, \pm 1, \pm 2, \dots$ . For the pure-exchange model, the analytical solution for topological configurations with a given value of  $Q$  was found by Belavin and Polyakov [38] (see also Ref. [59] for a more transparent approach). Due to the scale invariance of the exchange interaction in 2D, the energy of a skyrmion or antiskyrmion ( $Q = \pm 1$ ) with respect to the uniform state,  $\Delta E_{BP} = 4\pi J$ , does not depend on their size  $\lambda$ . In a continuous spin-field model, the conservation of the topological charge prevents skyrmions from decaying. Finite lattice spacing  $a$  breaks this invariance by adding a term of the order  $-(a/\lambda)^2$  to the energy, which leads to the skyrmion collapse [61]. This result was generalized for topological structures with any  $Q$  in Ref. [62].

In the presence of the DMI, only skyrmions, but not antiskyrmions, exist. To find a single-skyrmion spin configuration numerically, one can start with any state with  $Q = 1$  and perform energy minimization. The energy of a single skyrmion with respect to the uniform ferromagnetic state becomes negative for  $A$  large enough and  $|H|$  small enough, making the uniform state unstable to the creation of skyrmions. However, skyrmions compete with the laminar domains. A stable skyrmion solution exists in the field interval  $H_s \leq |H| \leq H_c$ . Below  $H_s \simeq 0.55A^2/J$  skyrmions become unstable against converting into a laminar domain structure [7]. Above  $H_c \simeq 0.97A^{3/2}/J^{1/2}$  skyrmions collapse [65]. The ratio of these fields is  $H_c/H_s \simeq 1.76 (J/A)^{1/2}$ . In this paper, we use the value  $A/J = 0.2$  which is typical for materials with nanoscale skyrmions, see, e.g. [49, 63]. In this case,  $H_c/J = 0.034$  and  $H_s/J = 0.022$ . Figure 1 shows a Bloch-skyrmion lattice in our model, Eq.(1), obtained by the numerical energy minimization at  $T = 0$  for  $A/J = 0.2$  and  $H/J = -0.025$ .

### B. Skyrmions as point particles

There is a short-range repulsion between skyrmions due to DMI [59]

$$U(r) \simeq F \exp\left(-\frac{r}{\delta_H}\right), \quad F \equiv 60J \left(\frac{A^2}{JH}\right)^2, \quad (3)$$

where  $r$  is the distance between the skyrmions' centers and  $\delta_H = a\sqrt{J/|H|}$  is the magnetic length. In sufficiently dense skyrmion lattices that we study here, this interaction dominates, whereas dipole-dipole repulsion of skyrmions can be neglected. This result allows considering a skyrmion lattice as a system of point particles with a repulsive interaction, Eq. (3), that is computationally easier than using the full model of lattice spins, Eq. (1).

The number of skyrmions  $N_S$  in the system at  $T = 0$  can be found by the minimization of the total energy. For a triangular lattice of skyrmions of the period  $a_S$  the unit-cell area is  $a_S^2\sqrt{3}/2$  and  $N_S$  can be expressed as

$$N_S = \frac{2}{\sqrt{3}} \frac{S}{a_S^2}, \quad (4)$$

where  $S$  is the total area of the system. Each skyrmion in the lattice interacts with its six nearest neighbors, whereas interactions with further neighbors can be neglected. The energy per skyrmion in the perfect lattice is

$$E_0 = \Delta E + 3F \exp\left(-\frac{a_S}{\delta_H}\right), \quad (5)$$

where  $\Delta E < 0$  is the skyrmion's core energy computed from the lattice-spins model [7]. The equilibrium state at  $T = 0$  can be obtained by the minimization of the total energy,  $\mathcal{E} = N_S E_0$  with respect to  $a_S$ , as described in Ref. [7]. For  $A/J = 0.2$  and  $H/J = -0.025$  one has  $\Delta E/J = -4.23$ ,  $\delta_H = 6.32a$ , and  $F/J = 154$  that results in  $a_S = 38.5a$ . The interaction energy between nearest neighbors  $U_0 = F \exp(-a_S/\delta_H) = 0.349J$  defines the scale for the skyrmion-lattice melting temperature  $T_m/J \simeq 0.12$ .

In the temperature range below as well as above melting the number of skyrmions in the system does not change because both annihilating a skyrmion or adding a skyrmion to the system requires overcoming large energy barriers [7]. In the processes under investigation  $\Delta E$  plays no role. One can consider metastable states in which  $N_S$  deviates from the value found by the energy minimization.

The quantity describing the orientation of the hexagon of the nearest neighbors of any skyrmion  $i$  in a 2D lattice is the local hexagonality

$$\Psi_i = \frac{1}{6} \sum_j \exp(6i\theta_{ij}). \quad (6)$$

Here the summation is carried out over the six nearest neighbors  $j$  of the skyrmion  $i$  (without the distance cut-off),  $\theta_{ij}$  is the angle between the  $ij$  bond and any fixed direction in the lattice. If  $\theta$  is counted from the direction of the  $x$ -axis (that is our choice), and two of the sides of the perfect hexagon coincide with the  $x$ -axis (as in the figures above), all terms in the sum are equal to 1, and thus  $\Psi_i = 1$ . We call this *horizontal* orientation of hexagons and label it by the red color. Rotation of the hexagons by  $30^\circ$  from the horizontal orientation results in the *vertical* orientation for which  $\Psi_i = -1$ . For any other orientation of a perfect hexagon,  $\Psi_i$  is a complex number of modulus 1. The angle  $\phi_i$  by which the hexagon  $i$  is rotated from its initial horizontal orientation is related to the phase angle  $\Theta_i$  in  $\Psi_i = |\Psi_i| e^{i\Theta_i}$  as  $\phi_i = \Theta_i/6$ .

At finite temperatures, orientations of the bonds fluctuate and the condition  $|\Psi_i| = 1$  no longer holds. The

quality of hexagons can be described by global hexagonality value defined as

$$V_6 \equiv \sqrt{\frac{1}{N_S} \sum_i |\Psi_i|^2}. \quad (7)$$

At temperatures well above the melting transition, when even the short-range order is completely destroyed, the orientations of the bonds and the angles  $\theta_{ij}$  become random. In this limit  $V_6 = \sqrt{1/6}$  as each particle has six nearest neighbors on average. The common orientation of hexagons in the lattice is described by the complex order parameter which is defined as local hexagonality averaged over the system:

$$\Psi = \frac{1}{N_S} \sum_i \Psi_i. \quad (8)$$

We compute the averages of these quantities over the Monte Carlo process obtaining

$$V_6 \equiv \left\langle \sqrt{\frac{1}{N_S} \sum_i |\Psi_i|^2} \right\rangle, \quad O_6 = \langle \Psi \rangle. \quad (9)$$

In addition, we define

$$G_6 = \sqrt{\langle |\Psi|^2 \rangle}. \quad (10)$$

For the hexagonality value one has  $V_6^2 > 0.5$  in the solid phase and  $V_6^2 < 0.5$  in the liquid phase. In the solid phase  $G_6 \cong |O_6|$ . In the liquid phase  $O_6$  reduces to zero by a long thermalization, whereas  $G_6$  remains finite and scales with  $1/\sqrt{N_S}$ . One can formally introduce the susceptibility

$$\chi = \frac{N_S}{3T} \left( \langle |\Psi|^2 \rangle - |\langle \Psi \rangle|^2 \right) \quad (11)$$

that contains both  $O_6$  and  $G_6$  and peaks at the melting/freezing point.

Similarly, one can compute the heat capacity via energy fluctuations:

$$C = \frac{d\langle E \rangle}{dT} = \frac{N_S}{T} \left( \langle E^2 \rangle - \langle E \rangle^2 \right) \quad (12)$$

with the energy per skyrmion given by

$$E = \Delta E + \frac{F}{2N_S} \sum_{ij} e^{-r_{ij}/\delta_H}, \quad (13)$$

where  $\Delta E$  does not contribute.

The quantity  $G_6$  also provides the information about orientational correlations in the system:

$$G_6^2 = \left\langle \frac{1}{N_S^2} \sum_{ij} \Psi_i \Psi_j^* \right\rangle = \frac{V_6^2}{N_S} \sum_{i-j} C_{6,i-j}, \quad (14)$$

where

$$C_{6,ij} = \frac{1}{V_6^2} \langle \Psi_i \Psi_j^* \rangle. \quad (15)$$

is the correlation function of the hexagonalities. Here the factor  $V_6^2$  is introduced to account for distortions of hexagons at nonzero temperatures and enforce  $C_{6,ii} = 1$ . If correlations are long, one can use continuous approximation

$$G_6^2 = \frac{V_6^2}{N_S} \int \frac{d^2r}{a_S^2 \sqrt{3}/2} C_6(r), \quad (16)$$

see Eq. (4). For  $C_6(r) = \exp[-(r/R_6)^p]$  one obtains

$$G_6^2 = \pi K_p \frac{2V_6^2 R_6^2}{N_S \sqrt{3} a_S^2} \implies \frac{R_6}{a_S} = \frac{G_6}{V_6} \sqrt{\frac{\sqrt{3} N_S}{2\pi K_p}}, \quad (17)$$

where  $K_1 = 2$  and  $K_2 = 1$ . Theory of critical phenomena considers correlation functions of the type  $C(r) \propto r^{2-d-\eta} e^{-r/R}$ , where  $d$  is the dimensionality of the space. With this Ansatz, one obtains  $G_6^2 \propto R_6^{2-\eta}$  and further the scaling relation  $\gamma = \nu(2-\eta)$ . The critical index  $\eta$  could be extracted from the behavior of the correlation function at criticality. However, in our case, there is a very steep temperature dependence at the melting/freezing point consistent with only a zero value of the critical index  $\beta$  for the orientational order parameter. Thus the state of the system at criticality is difficult to define and we are not using the critical Ansatz for the orientational CF.

### III. NUMERICAL METHOD

Throughout the paper, we consider the system with periodic boundary conditions (pbc) and sizes  $L_x \cong L_y$  compatible with the lattice without distortions (see Ref. [7] for details). We studied the small system having the linear size 30 in the SkL units  $a_S$  and containing  $N_S = 1080$  skyrmions, the medium system with the linear size 100 and 11600 skyrmions, and the large system with the linear size 300 and 104400 skyrmions.

To equilibrate the system at a particular temperature and a magnetic field, we used the classical Metropolis Monte Carlo (MC) method. Particles were successively moved by the random vector  $\Delta \mathbf{r}$  of the length  $|\Delta \mathbf{r}| = \text{dispmax} \times \text{rand}$ , where  $\text{rand}$  is a random real number in the range (0,1) and  $\text{dispmax}$  is the maximal displacement chosen automatically to maximize the effective displacement  $\text{dispeff} = 0.5 \text{dispmax} \times \text{acceptancerate}$ . It turns out that near and above melting the maximum of  $\text{dispeff}$  on  $\text{dispmax}$  is very flat and there is a tendency for  $\text{dispmax}$  to become comparable with  $a_S$ . Because of that, we introduced a limitation  $\text{dispmax} < \text{dispmaxmax} \equiv 0.3a_S$ . After each trial move, the energy change  $\Delta E_{\text{trial}}$  was computed and the move was accepted if  $\exp(-\Delta E_{\text{trial}}/T) > \text{rand}$ .

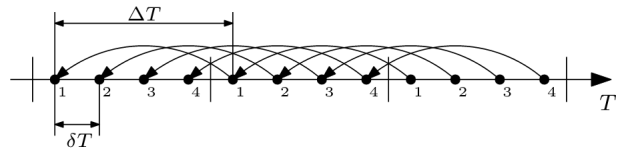


Figure 2. Parallelized relay computation – a four-core example with lowering temperature.

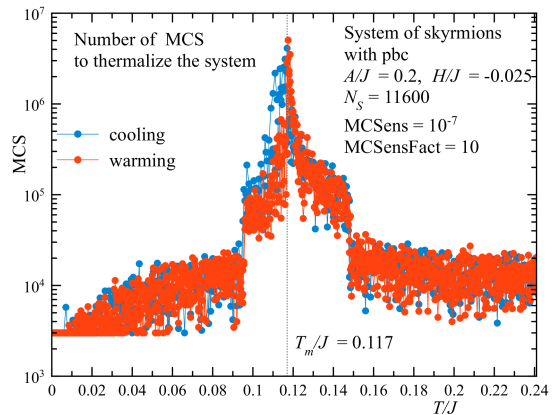


Figure 3. The number of MCS to thermalize the system strongly increases in the region of melting/freezing.

To properly deal with the interacting neighbors, we introduced the interaction cutoff  $r_{\text{cutoff}} = 0.95\sqrt{3}a_S$  that is just shy of the next-nearest distance in the triangular lattice,  $\sqrt{3}a_S$ , and subdivided the system into square bins of the size  $1.05r_{\text{cutoff}} + \text{dispmax}$ . For any skyrmion, interacting neighbors are looked up in the same bin and in the eight surrounding bins. This drastically reduces the procedure of finding the interacting neighbors that becomes not straightforward in the liquid phase where the particles are moving by large distances and the interacting neighbors change. The fast binning procedure was repeated after each Monte Carlo step (MCS), that is, after updating all particles in the system.

For computations in a broad region across the phase transition, it is very important to employ a Monte Carlo routine with an automated stopping criterion, as the number of MCS' necessary for equilibrating the system and measuring the physical quantities changes by orders of magnitude. Routines of this kind were used in some preceding work, e.g., in Ref. [7], but here we formulated the definitive algorithm. First, one chooses the control quantity (CQ) which is nonzero in both phases. One suitable quantity is the energy but here we use  $V_6$  defined by Eq. (7). The MC simulation is performed in blocks of MCBlock Monte Carlo steps, typical values being  $\text{MCBlock} = 50 - 100$ . After the completion of each block, the control quantity and other physical quantities are computed. The next computational parameter is  $\text{MCMass} < 1$  which defines the volume of the computed data used for data processing and finally for

the measurement. We form the lists of the most recent data of the length  $L = \text{Round}[\text{MCMass} \times N_{\text{val}}]$ , where  $N_{\text{val}} = \text{MCS}/\text{MCBlock}$  is the number of computed values of the physical quantities. That is, we use the fraction  $\text{MCMass}$  of all computed data, keeping the most recent results, while older results are discarded. Both  $N_{\text{val}}$  and  $L$  increase in the course of the simulation. Then, for the control quantity we compute the moving averages over the lists of length  $L$  using the triangular averaging kernel  $K_{L,i}$

$$\text{QCmean} = \sum_{i=1}^L K_{L,i} \text{QCList}_i, \quad \sum_{i=1}^L K_{L,i} = 1, \quad (18)$$

and form the list of the same length  $L$  from these averages,  $\text{CQmeanList}$ . The triangular averaging kernel yields a rather smooth list of data which is used to quantify the evolution of the control quantity. As  $K_{L,i}$  has a maximum at  $i = L/2$ , the values from the middle of the averaging interval  $L$  make the largest contribution.

We define the slope of the CQ per one MCS as

$$\text{CQ}_{\text{slope}} = \frac{\text{First}[\text{CQmeanList}] - \text{Last}[\text{CQmeanList}]}{L \times \text{MCBlock}} \quad (19)$$

Then we define the slope parameter

$$\text{SlopePar} = \text{CQ}_{\text{slope}} / (\text{CQ}_0 \times \text{MCSens}). \quad (20)$$

Here  $\text{CQ}_0$  is the typical value of the control quantity,  $\text{CQ}_0 = 1$  for  $V_6$ , and  $\text{MCSens}$  is the sensitivity of our Monte Carlo simulation, a very small number. We form the list of the most recent values of  $|\text{SlopePar}|$  of the same length  $L$ . The simulation is stopped when the mean value of this list becomes smaller than one – this is the most important new feature of the method.

One more improvement makes an accent on the critical region that is defined as the region where  $V_{6,\text{floor}} < V_6 < V_{6,\text{ceiling}}$ . We used  $V_{6,\text{floor}}^2 = 0.38$  and  $V_{6,\text{ceiling}}^2 = 0.69$ . These bracket the region in which melting/freezing takes place,  $V_6^2 \simeq 0.5$ . Whenever the computed value of  $V_6$  falls into this interval,  $\text{SlopePar}$  is multiplied by  $\text{MCSensFact} = 10$ . As a result, the stopping criterion becomes more stringent in the critical region than otherwise. The method always converges, even in the case of slow large-amplitude stationary fluctuations because of the increasing  $L$  in the definition of  $\text{CQ}_{\text{slope}}$ , Eq. (19). After stopping, the latest of the moving averages of the control quantity,  $\text{Last}[\text{CQmeanList}]$ , is output. For the other quantities, the mean values over the lists of  $L$  most recent values are output. The smaller the parameter  $\text{MCSens}$ , the longer simulation is done and the more extensive is the averaging of the computed quantities. Fig. 3 illustrates the number of MCS needed to achieve thermalization for the system of 11600 skyrmions with  $\text{MCSens} = 10^{-7}$ . The number of MCS increases in the critical region and peaks at the melting/freezing point  $T/J = 0.117$ . Since the main computing time is spent

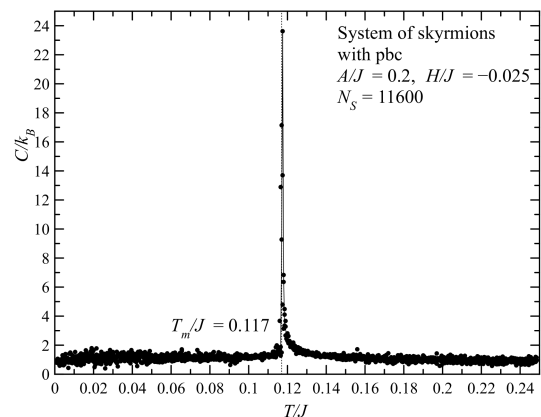
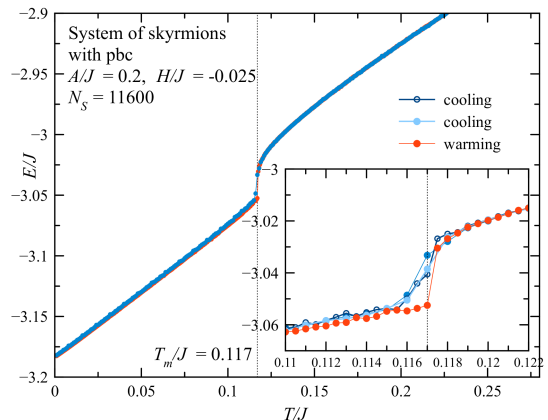


Figure 4. The temperature dependences of the energy per skyrmion (Upper panel. Inset shows the magnification of the transition region with a negligible hysteresis) and the heat capacity per skyrmion obtained from the energy fluctuations, Eq. (12) (Lower panel).

near melting/freezing anyway, one can make computations in a broad range of  $T$  with the same  $T$ -interval. One does not need to rarify the points away from the phase transition region because these points cost a relatively short computing time.

The Monte Carlo algorithm presented above is superior to the version used in Ref. [7]. Whereas the number of MCS done in Ref. [7] does not exceed one million, here it goes up to several millions that provides a better thermalization and averaging of stationary fluctuations near the transition. The main focus here is on the system with  $\sim 10^4$  skyrmions which is sufficiently large to study thermodynamics. Here in computing temperature dependences of the quantities, we used a finer  $T$ -grid than in Ref. [7].

Computations were performed with Wolfram Mathematica using compilation of the core routines such as Monte Carlo and those computing the physical quantities. Dependences on  $T$  and  $H$  were computed in parallelized cycles using the number  $N_{\text{cores}}$  of the available processor cores and the so-called *relay* method (see Fig.

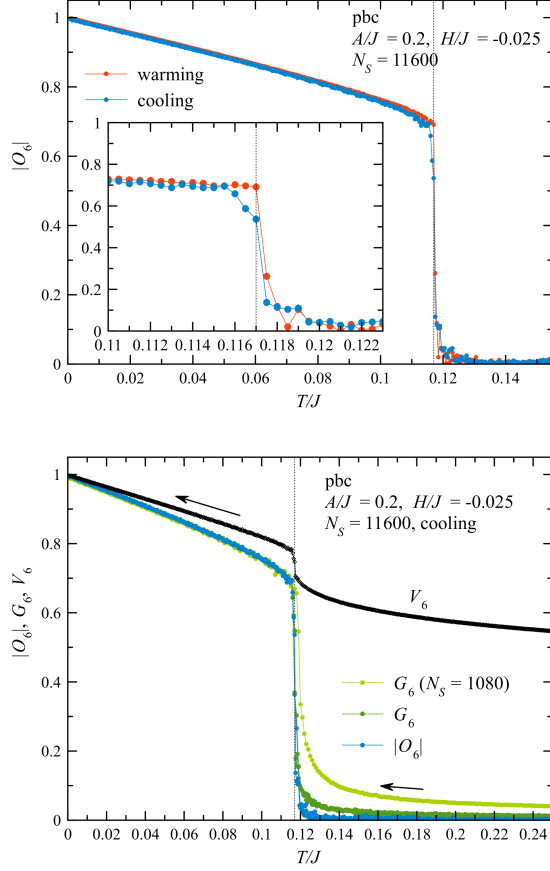


Figure 5. Orientational order parameter  $O_6$  vs temperature (Upper panel. Inset shows a jump with a negligible hysteresis) and the temperature dependence of the orientational quantities on cooling (Lower panel).

2) in which the next  $T$ -point within the same thread uses the previously obtained state as the initial condition. With the interval between the neighboring  $T$ -points being  $\delta T$ , the interval between those within the same thread is  $\Delta T = N_{\text{cores}} \delta T$  that is sufficiently small if  $\delta T$  is small and  $N_{\text{cores}}$  is not too large. We mainly used 8 cores for these computations. The initial conditions were perfect lattice or random placement of skyrmions.

#### IV. THERMODYNAMICS OF MELTING AND FREEZING

We have found that in our case SkL melting/freezing occurs according to the grain scenario [25, 26] via only one melting/freezing transition between solid and liquid phases. In Ref. [7] we concluded that this phase transition is first order because the orientational order parameter  $O_6$  jumped to zero at the melting temperature. However, as we show here, this transition possesses features of second-order transitions such as divergent heat capacity and susceptibility. These are more reliable in

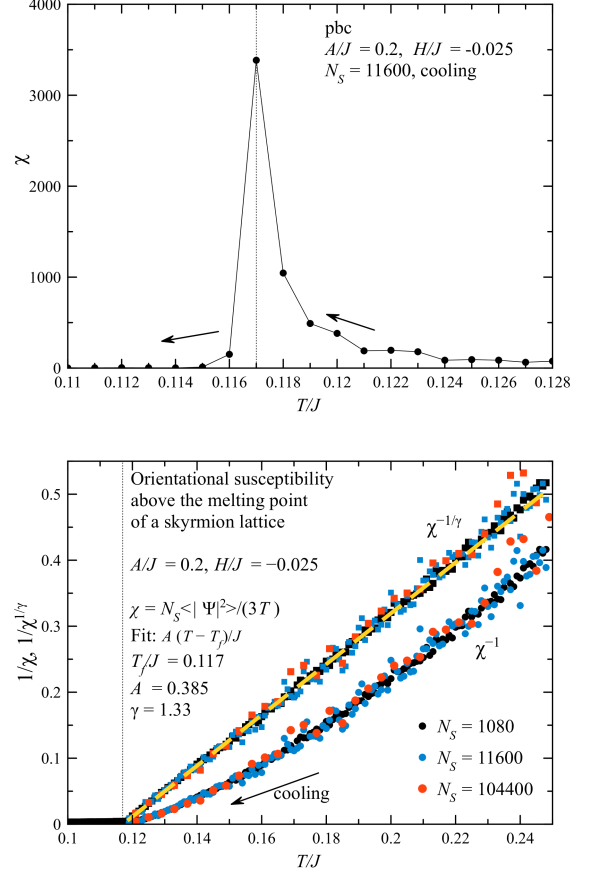


Figure 6. Upper panel: Susceptibility associated with the orientational order peaks at the melting/freezing transition. Lower panel: Critical dependence of the inverse susceptibility above freezing.

the determination of the order of the transition than a jump of the order parameter because in simulations it is difficult to distinguish a jump from a very steep dependence.

Melting/freezing is a very slow process including slow relaxation and slow large-amplitude stationary fluctuations. Large areas of the system are melting and freezing again. Nevertheless, for the system of  $10^4$  skyrmions thermodynamic averages at equilibrium can be obtained by the Metropolis Monte Carlo within  $10^6 - 10^7$  Monte Carlo steps (MCS), see Fig. 3. With a full thermalization, there is practically no hysteresis and the melting temperature  $T_m$  is practically equal to the freezing temperature  $T_f$ . Hysteresis is observed in the cases of incomplete equilibration, for instance, if the stopping criterion for thermalization is too liberal or if the temperature changes at a too high rate.

Larger systems, such as  $10^5$  skyrmions, tend to freeze into a polycrystal state which then evolves very slowly toward the monocrystal state, see Sec. VI. This process for large systems is even slower than melting/freezing.

The energy per particle  $E$  shows a singularity just

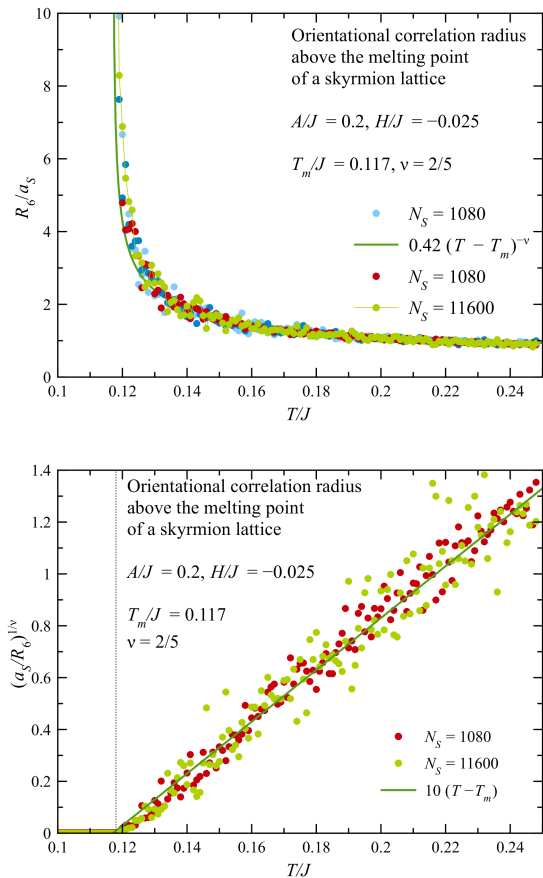


Figure 7. Orientational correlation length  $R_6$  computed using Eq. (17).

above the transition, see Fig. 4. The heat capacity  $C$  per particle obtained from the energy fluctuations, Eq. (12), and shown in the lower panel of Fig. 4 peaks in this region, although the numerical data does not allow to reliably infer its critical behavior. The singularity of  $C$  is not a robust power law and resembles a logarithmic divergence. In the low-temperature region the analytical result is  $C = k_B$  that is reproduced in the simulation.

The orientational order parameter  $O_6$  exhibits a linear dependence at low temperatures (that is typical for classical systems) and a jump or an unresolved very steep dependence at melting/freezing, see Fig. 5. The average hexagonality value  $V_6$  decreases with the temperature and shows a steep descent just above the melting/freezing point (lower panel of Fig. 5). The orientational parameter  $G_6$  is smooth above melting and decreases with the temperature and the system size. In the skyrmion-liquid phase,  $G_6 \gg O_6$ , while in the solid phase  $G_6 \cong O_6$ , thus the susceptibility has a peak at melting/freezing, as is shown in the upper panel of Fig. 6. To obtain this plot, we used  $\text{MCSense} = 10^{-8}$  with  $\text{MCSensFact} = 10$ . The inverse susceptibility computed for the systems of  $10^3$ ,  $10^4$ , and  $10^5$  skyrmions and shown in the lower panel of

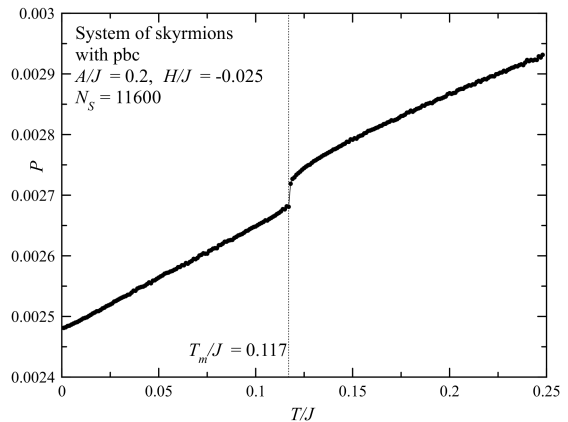


Figure 8. Temperature dependence of the pressure in the skyrmion matter.

the same figure has an apparent critical behavior with the critical index  $\gamma \simeq 1.33$ .

Fig. 7 shows the temperature dependence of the orientational correlation length above melting, obtained from  $G_6$ , Eq. (10). The exponential Ansatz for the orientational correlation function, see Eq. (17), yields a critical divergence of the correlation length  $R_6/a_S \simeq 0.42[(T - T_m)/J]^{-\nu}$  with  $\nu = 2/5$ .

The system of skyrmions is a system with a pure repulsion, thus it is always under pressure that keeps the system together. One can calculate pressure as the force acting perpendicularly across any line in the system per unit length of this line. For a perfect lattice at  $T = 0$  taking into account only the six nearest neighbors one obtains

$$P = \frac{\sqrt{3}f}{a_S}, \quad f = \left. \frac{dU(r)}{dr} \right|_{r=a_S} = \frac{F}{\delta_H} \exp\left(-\frac{a_S}{\delta_H}\right). \quad (21)$$

where  $f$  is the magnitude of the repulsion force between the two skyrmions. The temperature dependence of the pressure shown in Fig. 8 is similar to that of the energy, Fig. 4. In particular, melting causes a steep increase of the pressure.

Usually pressure is computed for different concentrations of particles. For a system of skyrmions, it is more convenient to control pressure by the applied magnetic field as the repulsion energy depends on  $H$  via the magnetic length  $\delta_H = \sqrt{J/|H|}$  and the exponential prefactor  $F$ . Increasing the field strength reduces the interaction and causes melting of the skyrmion lattice, as shown in Fig. 9. The dependence on  $H$  is less steep than the temperature dependence, and one can see that the phase transition on  $H$  is clearly continuous.

Increasing the strength of the magnetic field reduces the pressure in the system. However, melting of the skyrmion lattice increases pressure that can create a Mayer-Wood loop. This loop is difficult to see, though, as it is masked by a strong regular part of the dependence

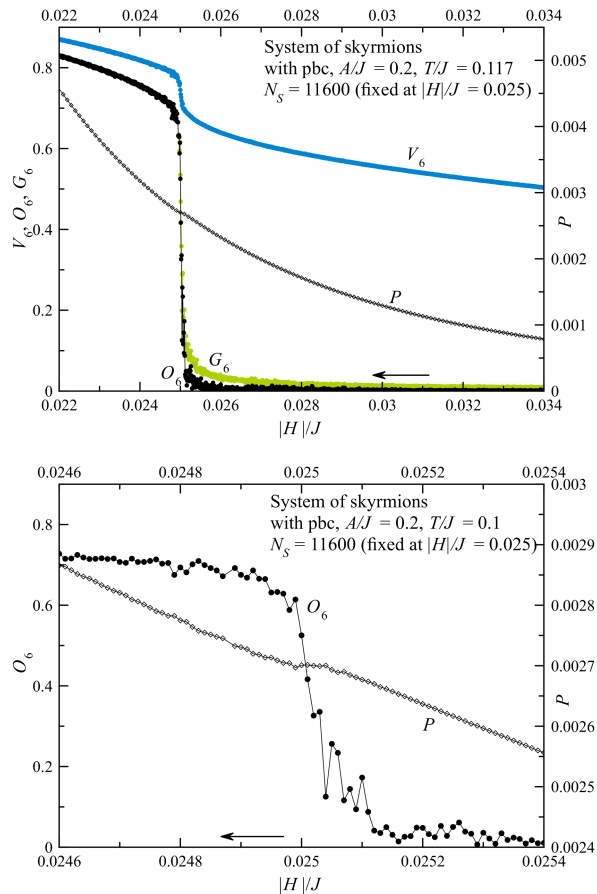


Figure 9. Freezing of the skyrmion lattice on decreasing the strength of the magnetic field is a continuous transition with a small Mayer-Wood loop for the pressure.

$P(H)$  that is much more pronounced than the  $P(T)$  dependence. Still, one can see a small Mayer-Wood loop in the lower panel of Fig. 9.

## V. SPONTANEOUS EMERGENCE OF LATTICE DEFECTS AND FORMATION OF GRAINS

The process of melting of a skyrmion lattice goes via spontaneous formation of grains with different orientation of hexagons, as suggested by Chui (see Fig. 10). Grains are separated from each other by the lines where the lattice is broken and dislocations are clustered. Clustered dislocations can be identified as skyrmions having the number of Delaunay nearest neighbors different from six. Near the melting/freezing temperature, in the course of the Monte Carlo simulation, grains appear and disappear, grain boundaries move back and forth. This process is very long. Above the melting temperature, the tendency of increasing the number of differently oriented grains dominates. Below this temperature, to the contrary, grains tend to coalesce into bigger ones, until there is a uniform orientation of hexagons in the system. We

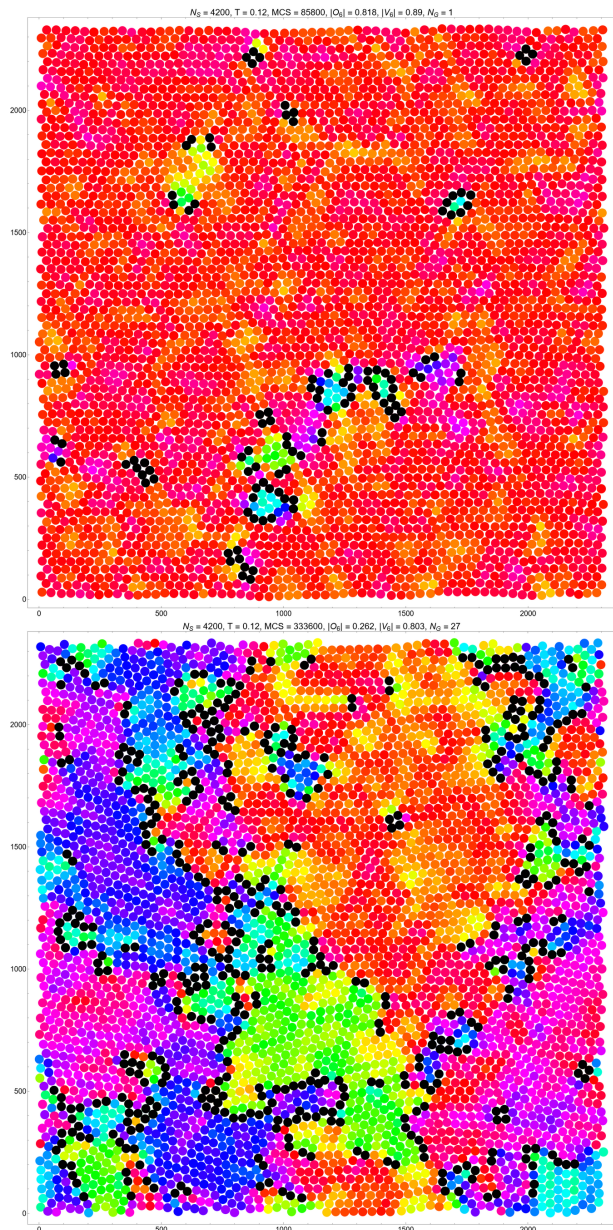


Figure 10. Early and advanced stages of melting of the SkL slightly above the melting temperature. The process goes via formation of grains with a different orientation of hexagons (color coded). Grains are separated by lines of dislocations shown in black.

do not observe the so-called “unbinding” of dislocations or disclinations – with increasing the temperature lattice defects emerge bound in clusters.

Fig. 11 shows the temperature dependence of the concentration of lattice defects: dislocations, free dislocations, and free disclinations. Although dislocations are defined via the Burgers vector, at nonzero temperatures, when the lattice is deformed, it is more convenient to look at the Delaunay graph showing the number of nearest neighbors for each particle. Particles having five of seven nearest neighbors are disclinations. We count free

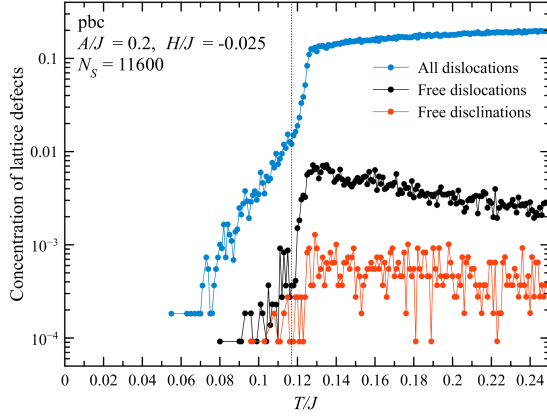


Figure 11. Temperature dependence of the number of lattice defects across the melting transition.

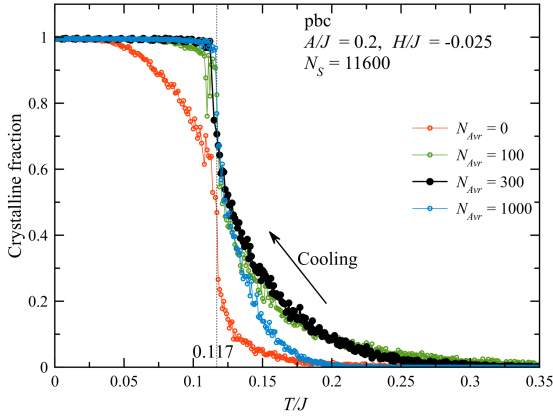


Figure 12. Crystal fraction vs temperature for different lengths of positional averaging.

disclinations which are separated by a distance of least  $2a_S$  from other defects. A pair of 5- and 7-disclinations separated by the distance of order  $a_S$  form a dislocation. Again, we count free dislocations which are separated by a distance of at least  $2a_S$  from other defects. Also we count all dislocations, including clustered ones. As can be seen, only a small fraction of lattice defects are free while the majority of them are clustered. Moreover, the number of free dislocations and disclinations decreases with temperature above  $T_m$ . This happens because the total number of dislocations increases and it becomes difficult to find a place not close to any of them.

As the temperature increases beyond the melting temperature, the regions between the grains, where the lattice is broken, become wider. Here the skyrmion matter become liquid, and the fraction of the liquid phase increases with temperature. This can be quantified as follows. The temperature dependence  $V_6(T)$  shown in the lower panel of Fig. 5 suggests using the criterion  $V_6^2 > 0.5$  for solid and  $V_6^2 < 0.5$  for liquid. Around

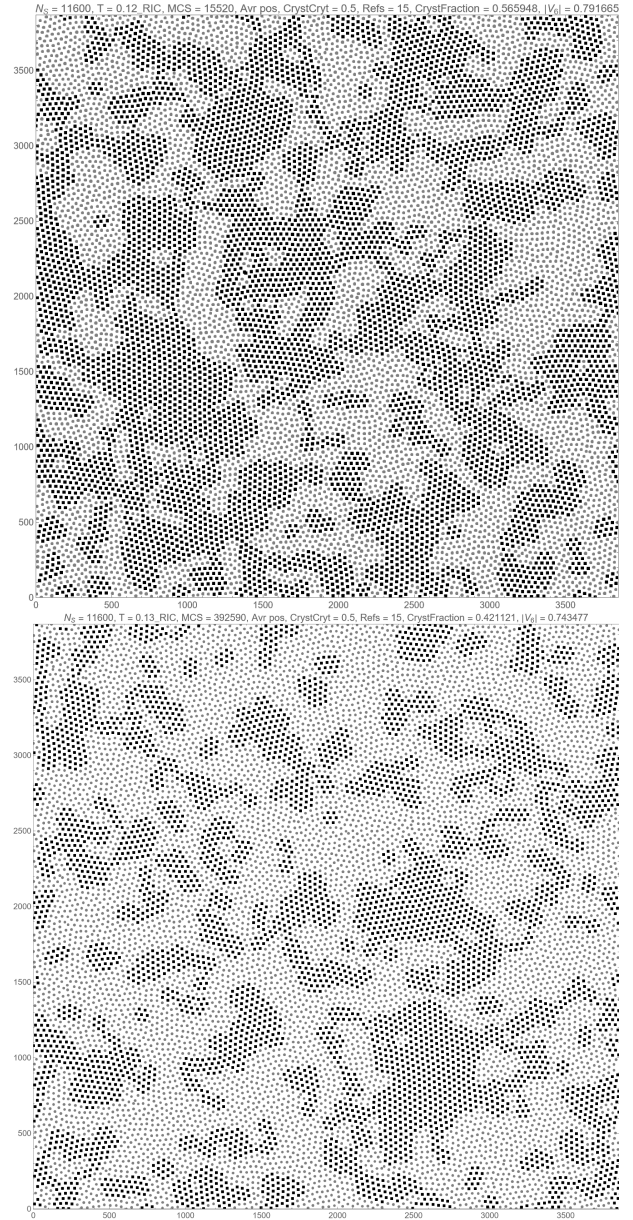


Figure 13. Skyrmion matter after positional averaging at  $T/J = 0.12$  and  $0.13$ . Skyrmions belonging to the solid part are shown by black points and those belonging to the liquid part are shown by gray points.

the melting/freezing transition, there are regions of both types, and by computing their areas (or the numbers of skyrmions in them) one can define the crystalline fraction. This quantity is shown in red in Fig. 12. One can see that there is some crystalline fraction above melting as well as some liquid fraction below melting. However, besides slow processes of grain dynamics, there is a fast quasi-harmonic motion of the particles that creates lattice deformations decreasing the hexagonality  $V_6$ . To make a more reliable separation between liquid and solid parts of the system, one can perform a short averaging of skyrmions' positions over the Monte Carlo process – so

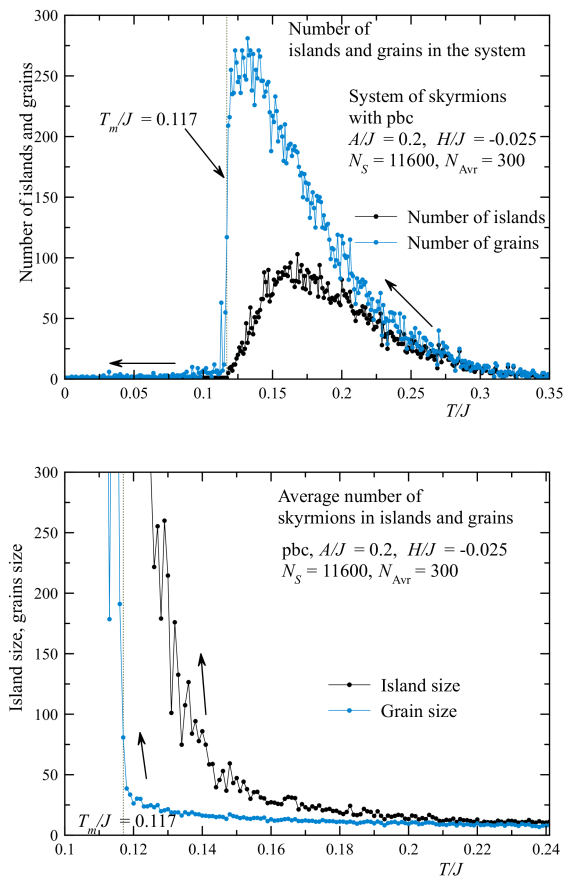


Figure 14. Temperature dependence of the number of islands and grains (upper panel) and of the average size of islands and grains (lower panel).

short that it averages out the quasiharmonic motion but does not affect the slow grain dynamics. The corresponding results are shown in Fig. 12 for several different values of the averaging Monte Carlo steps  $N_{avr}$  performed after the system was thermalized. As the result of positional averaging, the liquid part below  $T_m$  disappears completely that confirms the hypothesis about its origin as fully due to the quasi-harmonic motion. The crystalline part above melting increases as well for the same reason. However, too long averaging begins to reduce the crystalline part at higher temperatures because here grain dynamics becomes faster. For revealing grains in the melt, there is an optimum length of the averaging cycle  $N_{avr} = 100 - 300$  MCS, as can be seen in Fig. 12.

One can enumerate the islands of solid within the liquid with the help of the connected-component labeling algorithm. In this way, one can also find the average island size (the average number of skyrmions in the island). This algorithm can be generalized making it resolved with respect to the orientation of hexagons. In the following we call regions of solid with an unresolved hexagon orientation “island” and those with a resolved orientation “grains”. One island can consist of several

grains, so there are more grains than islands. Some grains are separated from each other by dislocations-rich grain boundaries. There are also continuous changes of grain orientations that do not lead to creation of dislocations. To define grains in this situation, we set intervals of  $10^\circ$  for hexagon orientations. When the orientation changes by more than 10 degrees, this is considered as another grain. As the full interval of hexagon orientations is  $60^\circ$ , there are only six different grain orientations that we take into account here.

Temperature dependences of the number of islands and grains, as well as that of the average island and grain size, is shown in Fig. 14. Well above  $T_m$  everything is liquid and the number of islands and grains goes to zero. With lowering the temperature, grains are formed and their number increases. However, with a further lowering temperature, islands begin to coalesce, and their number decreases after reaching a maximum. In this region, the number of grains still increases as the big coalesced islands consist of many grains with different orientations. Finally, at the freezing point all grains acquire the same orientation and become one grain, that is, a monocrystal. Below freezing, there is one island and one grain. The size of islands and grains in the lower panel of Fig. 14 monotonically increases with lowering temperature starting from its minimal value of six particles in the island or grain. Below  $T_m$  the island size and the grain size are equal to the number of skyrmions in the system.

It should be noted that the state with grains of solid within the melt is not a mixed state because grains are volatile and there is no second temperature, above the melting/freezing temperature, at which grains completely disappear. In most of the temperature range, except for a close vicinity of  $T_m$ , grains are very small to be considered as a thermodynamically stable phase. Rather, grains are correlated regions above the ordering transition, precursors of the emerging ordering. The average grain size gives an estimation of the correlation length above the transition.

## VI. NONEQUILIBRIUM EFFECTS IN THE POLYCRYSTALLINE STATE

Large systems of skyrmions on lowering the temperature freeze into a polycrystalline state. The pure system with periodic boundary conditions that we are studying here then tends to evolve very slowly towards the monocrystalline state via the motion of boundaries between differently oriented grains. If there is only one flat boundary between the two large grains, the system will stay in this state forever. Also even a weak pinning or the effect of boundaries will prevent the system from reaching the monocrystalline state. In particular, a square system with rigid boundaries is a frustrated system because differently oriented rigid boundaries favor different orientations of hexagons.

To elucidate the evolution of the polycrystalline state,

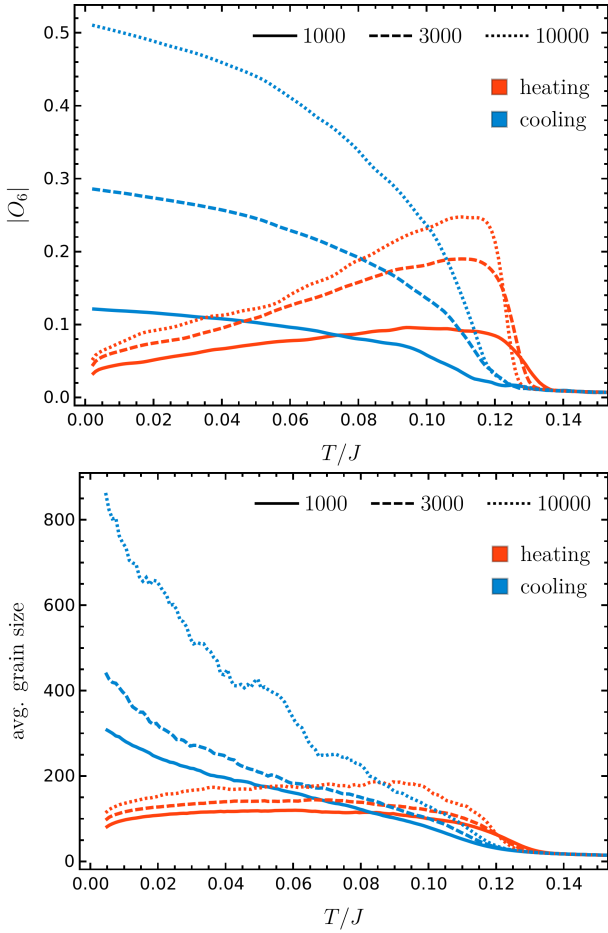


Figure 15. Nonequilibrium effects on heating and cooling of the skyrmion lattice (with the initial random placement of skyrmions) have some similarity to field-cooled and zero-field-cooled phenomena observed in arrays of magnetic particles. The data was obtained on the system of 104400 skyrmions by stepwise increasing and decreasing  $T$  with  $\delta T/J = 0.001$  and the number of MCS at each temperature 1000, 3000, and 10000. Upper panel: the orientational order parameter is reduced because the state is polycrystalline. Lower panel: the average grain size (the number of skyrmions in the grain) in the polycrystalline state.

we performed stimulated annealing experiments on the large system with 104400 skyrmions by stepwise increasing and decreasing the temperature with the  $T$ -step  $\delta T/J = 0.001$  and the number of MCS at each temperature 1000, 3000, and 10000. In the last case, the total number of MCS done in changing the temperature between zero and  $T/J = 0.1$  is  $10000 \times 0.1/0.001 = 10^6$ . Both for warming and cooling, we start with a random placement of skyrmions. At  $T = 0$ , the system relaxes into a metastable state with small differently oriented grains and thus a small value of the orientational order parameter  $O_6$ . The process of grains coarsening is very slow at low temperatures. With increasing  $T$ , the coarsening goes faster and  $|O_6|$  increases up to the point of melting before it finally goes down. This behavior has a

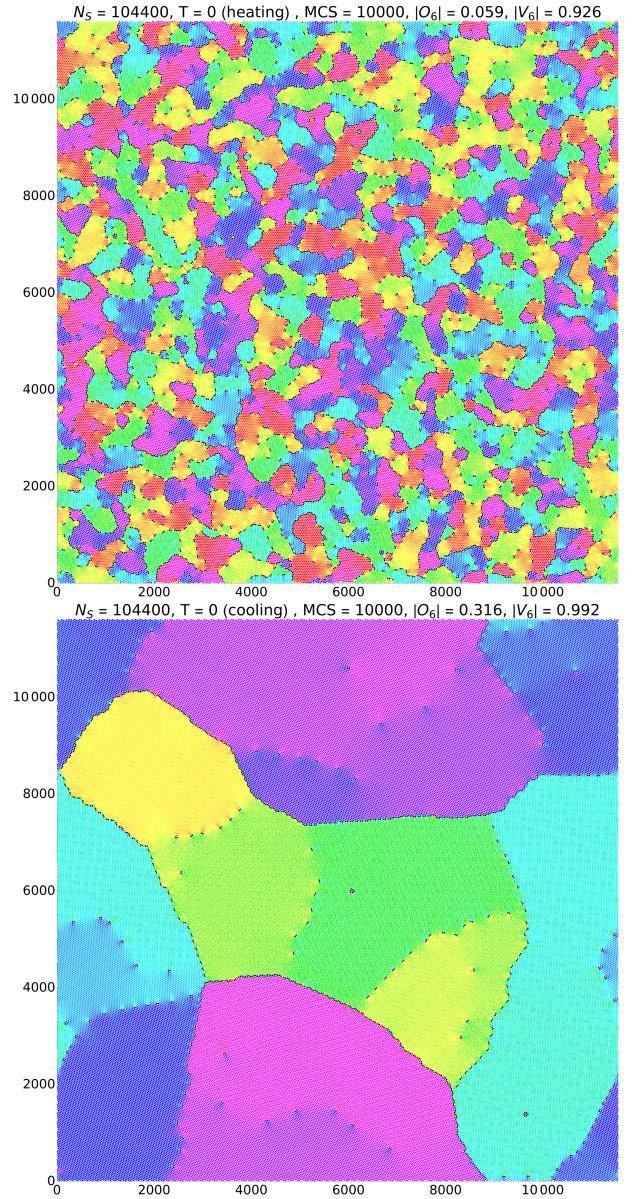


Figure 16. The polycrystalline state in the system of 104400 skyrmions at  $T = 0$  with 10000 MCS per temperature point. The hexagon orientation is color-coded as above. Skyrmions having 5 or 7 Delaunay nearest neighbors are shown in black. Upper panel: small grains obtained by quenching from the initial state with a random placement of skyrmions. Such states are then warmed up that leads to coarsening of grains. Lower panel: Large grains obtained by gradual lowering of the temperature.

similarity to that observed in the zero-field-cooled experiments on magnetic systems. However, there is no analog of the applied field that causes increasing of the magnetization with increasing  $T$ , and  $|O_6| \propto \sqrt{\text{GrainSize}/N_S}$  decreases with the system's size.

A more suitable quantity characterizing the polycrystalline state is the average grain size, as defined in the preceding section. This quantity does not depend on

the system size for large systems. As the grain size can be rather big, studying the polycrystalline state requires large systems. Fig. 15 shows the temperature dependences of  $|O_6|$  and the grain size in the system of 104400 skyrmions. With increasing the number of MCS done at each  $T$ -point, both  $|O_6|$  and the grain size increase, although much more MCS is needed to reach the monocrystalline state with  $|O_6| = 1$  in the limit  $T \rightarrow 0$  and the grain size equal to the system size.

Examples of the states of the system of  $N_S = 104400$  with 10000 MCS per temperature point at  $T = 0$  are shown in Fig. 16. The upper panel shows small grains obtained by quenching from the initial state with a random placement of skyrmions. Such states are then warmed up that leads to the coarsening of grains, see warming curves in Fig. 15. The lower panel shows large grains obtained by gradual lowering the temperature, see cooling curves in Fig. 15.

## VII. CONCLUSIONS

Skyrmion lattices provide another field for testing the predictions of the theory of 2D melting. They present an advantage over systems of particles due to the possibility of continuously changing interaction between skyrmions by changing the external magnetic field. Here we performed comprehensive Monte-Carlo studies of the melting of 2D skyrmion lattice. The temperature and the field dependence of the positional and orientational order parameters have been computed in systems of various sizes ranging from  $10^3$  to  $10^5$  skyrmions, and images of skyrmion lattices near the melting transition have been obtained. Skyrmions repel each other with a force

that goes down exponentially with the distance between the skyrmions. The decay length is determined by the magnetic field. When the system is small enough, thermal equilibrium is achieved, and we observe a sharp reversible solid-liquid transition without an intermediate hexatic phase. Larger systems fail to achieve thermal equilibrium and exhibit hysteresis on cycling the temperature. For both equilibrium and non-equilibrium systems we find that the melting and freezing transitions occur via the formation of grains with different orientations of hexagonal axes. The departure from a simple picture of a transition caused by the unbinding of dislocation and disclination pairs is due to the clustering of the defects into the grain boundaries. We observe the granular structure on both heating and cooling, with the only difference that in the liquid phase it corresponds to the grains of a fluctuating shape while in the solid phase it corresponds to a more stable polycrystal. On cooling the fluctuating grains freeze into a polycrystal which behaves similarly to ordinary crystals on annealing. Our findings show that the scenarios of melting driven by the unbinding of free defects and melting driven by the formation of grains are likely to be the two limiting cases of a more complex scenario in which many-body interaction between the defects plays a crucial role.

## VIII. ACKNOWLEDGMENTS

This work was supported by Grant No. DE-FG02-93ER45487 funded by the U.S. Department of Energy, Office of Science, and Grant No. FA9550-24-1-0090 funded by the Air Force Office of Scientific Research.

- 
- [1] M. C. Ambrose and R. L. Stamps, Melting of hexagonal skyrmion states in chiral magnets, *New Journal of Physics* **15**, 053003-(14) (2013). I, I
  - [2] Y. Nishikawa, K. Hukushima, and W. Krauth, Solid-liquid transition of skyrmions in a two-dimensional chiral magnet, *Physical Review B* **99**, 064435 (2019). I
  - [3] J. Zázvorka, F. Dittrich, Y. Ge, N. Kerber, K. Raab, T. Winkler, K. Litzius, M. Veis, P. Virnau, and M. Kläui, Skyrmion lattice phases in thin film multilayers, *Advanced Functional Materials* **30**, 2004037-(8) (2020). I
  - [4] P. Huang, T. Schönenberger, M. Cantoni, L. Heinen, A. Magrez, A. Rosch, F. Carbone, and H. M. Rønnow, Melting of a skyrmion lattice to a skyrmion liquid via a hexatic phase, *Nature Nanotechnology* **15**, 761-767 (2020). I
  - [5] P. Baláž, M. Paściak, and J. Hlinka, Melting of Néel skyrmion lattice, *Physical Review B* **103**, 174411-(8) (2021). I
  - [6] A. R. C. McCray, Yue Li, R. Basnet, K. Pandey, J. Hu, D. P. Phelan, X. Ma, A. K. Petford-Long, and C. Phatak, Thermal hysteresis and ordering behavior of magnetic skyrmion lattices, *Nanoletters* **22**, 7804-7810 (2022). I
  - [7] D. A. Garanin and E. M. Chudnovsky, Polyhexatic and polycrystalline states of skyrmion lattices, *Physical Review B* **107**, 014419-(17) (2023). I, II A, II B, II B, III, III, III, IV
  - [8] P. Meisenheimer, H. Zhang, D. Raftrey, X. Chen, Y.-T. Shao, Y.-T. Chan, R. Yalisove, R. Chen, J. Yao, M. C. Scott, W. Wu, D. A. Muller, P. Fischer, R. J. Birgeneau, R. Ramesh, Ordering of room-temperature magnetic skyrmions in a polar van der Waals magnet, *Nature Communications* **14** 3744-(9) (2023). I, I
  - [9] J. M. Kosterlitz, Kosterlitz-Thouless physics: a review of key issues, *Reports on Progress in Physics* **79** 026001-(60) (2016). I
  - [10] V. N. Ryzhov, E. A. Gaidul, E. E. Tareeva, Y. D. Fomin, and E. N. Tsiok, Melting scenarios of two-dimensional systems: Possibilities of computer simulation, *Journal of Theoretical and Experimental Physics (JETP)* **137**, 125-150 (2023). I
  - [11] R. E. Peierls, Remarks on transition temperatures, *Helvetica Physica Acta* **7**, 81-83 (1934). I
  - [12] N. D. Mermin and H. Wagner, 1966 Absence of ferromagnetism or antiferromagnetism in one or two-

- dimensional isotropic Heisenberg models, *Physical Review Letters* **17** 1133-1136 (1966). I
- [13] P. C. Hohenberg, Existence of long-range order in one and two dimensions *Physical Review* **158**, 383-386 (1967). I
- [14] B. J. Adler and T. E. Wainwright, Phase transition in elastic disks, *Physical Review* **127**, 369-361 (1962). I
- [15] R. S. Kagiwada, J. C. Fraser, I. Rudnick, and D. Bergman, Superflow in helium films, *Physical Review Letters* **22**, 338-342 (1969). I
- [16] V. L. Berezinskii, Destruction of long range order in one-dimensional and two-dimensional systems having a continuous symmetry group. I. Classical systems, *Journal of Experimental and Theoretical Physics (JETP)* **32**, 493-500 (1971). I
- [17] J. M. Kosterlitz and D. J. Thouless, Long range order and metastability in two-dimensional solids and superfluids, *Journal of Physics C: Solid State Physics* **5** L124-L126 (1972); Ordering, metastability and phase transitions in two-dimensional systems, *Journal of Physics C: Solid State Physics* **6** 1181-1203 (1973). I
- [18] D. J. Bishop and J. D. Reppy, Study of the superfluid transition in two-dimensional  $^4\text{He}$  films *Physical Review Letters* **40** 1727-1730 (1978); *Physical Review B* **22** 5171-5185 (1980). I
- [19] B. I. Halperin and D. R. Nelson, Theory of two-dimensional melting, *Physical Review Letters* **41**, 121-124 (1978). I
- [20] D. R. Nelson and B. I. Halperin, Dislocation-mediated melting in two dimensions, *Physical Review B* **19**, 2457-2483 (1979). I
- [21] A. P. Young, Melting and the vector Coulomb gas in two dimensions, *Physical Review B* **19**, 1855-1866 (1979). I
- [22] J. Q. Broughton, G. H. Gilmer, and J. D. Weeks, Molecular-dynamics study of melting in two dimensions: Inverse-twelfth-power interaction, *Physical Review B* **25**, 4651-4669 (1982). I
- [23] F. Lindemann, About the Calculation of Molecular Own Frequencies, *Zeitschrift für Physik* **11**, **14**, 609-612 (1910). I
- [24] S. A. Khrapak, Lindenmann melting criterion in two dimensions, *Physical Review Research* **2**, 012040(R)-(6) (2020). I
- [25] S. T. Chui, Grain-boundary theory of melting in two dimensions, *Physical Review Letters* **48**, 933-935, (1982); *Physical Review B* **28**, 178-194 (1983). I, I, IV
- [26] Y. Saito, Monte Carlo studies of two-dimensional melting: Dislocation vector systems, *Physical Review B* **26**, 6239-6253, (1982). I, I, IV
- [27] D. S. Fisher, B. I. Halperin, and R. Morf, Defects in the two-dimensional electron solid and implications for melting, *Physical Review B* **20**, 4692-4712 (1979). I
- [28] W. Janke and H. Kleinert, From first-order to two continuous melting transitions: Monte Carlo Study of a new 2D lattice-defect model, *Physical Review Letters* **61**, 2344-2347 (1988); Erratum *Physical Review Letters* **62**, 608 (1989). I
- [29] E.M. Chudnovsky, Structure of a solid film on an imperfect surface, *Physical Review B* **33**, 245-250 (1986). I
- [30] E.M. Chudnovsky, Hexatic vortex glass in disordered superconductors, *Physical Review B* **40**, (R)11355-11367 (1989). I
- [31] C. A. Murray, P. L. Gammel, D. J. Bishop, D. B. Mitzi, and A. Kapitulnik, Observation of a hexatic vortex glass in flux lattices of the high- $T_c$  superconductor  $\text{Bi}_{2.1}\text{Sr}_{1.9}\text{Ca}_{0.9}\text{Cu}_2\text{O}_{8+\delta}$ , *Physical Review Letters* **64**, 2312-2315 (1990); D. G. Grier, C. A. Murray, C. A. Bolle, P. L. Gammel, D. J. Bishop, D. B. Mitzi, and A. Kapitulnik, Translational and bond-orientational order in the vortex lattice of the high- $T_c$  superconductor  $\text{Bi}_{2.1}\text{Sr}_{1.9}\text{Ca}_{0.9}\text{Cu}_2\text{O}_{8+\delta}$ , *Physical Review Letters* **66**, 2270-2273 (1991). I
- [32] H. H. Günberg, P. Keim, K. Zahn, and G. Maret, Elastic behavior of a two-dimensional crystal near melting, *Physical Review Letters* **93** 255703-(4) (2004). I
- [33] J. Zanghellini, P. Keim, and H. H. von Grünberg, The softening of two-dimensional colloidal crystals, *Journal of Physics: Condensed Matter* **17** S3579-S3586 (2005). I
- [34] J. Dietel and H. Kleinert, Triangular lattice model of two-dimensional defect melting, *Physical Review B* **73**, 024113-(13) (2006). I
- [35] S. C. Kapfer and W. Krauth, *Physical Review Letters* **114**, 035702-(5) (2015).
- [36] J. A. Anderson, J. Antonaglia, J. A. Millan, M. Engel, and S. Glotzer, Shape and symmetry determine two-dimensional melting transitions of hard regular polygons, *Physical Review X* **7**, 021001-(14) (2017).
- [37] E. N. Tsiok, Y. D. Fomin, E. A. Gaiduk, E. E. Tareyeva, V. N. Ryzhov, P. A. Libet, N. A. Dmitryuk, N. P. Kryuchkov, and S. O. Yurchenko, *Journal of Chemical Physics* **156**, 114703-(11) (2022). I
- [38] A. A. Belavin and A. M. Polyakov, Metastable states of two-dimensional isotropic ferromagnets, *Pis'ma Zh. Eksp. Teor. Fiz.* **22** 503-506 (1975) [*JETP Lett.* **22**, 245-247 (1975)]. I, II A, II A
- [39] N. Nagaosa and Y. Tokura, Topological properties and dynamics of magnetic skyrmions, *Nature Nanotechnology* **8**, 899-911 (2013). I
- [40] X. Zhang, M. Ezawa, and Y. Zhou, Magnetic skyrmion logic gates: conversion, duplication and merging of skyrmions, *Scientific Reports* **5**, 9400-(8) (2015).
- [41] G. Finocchio, F. Büttner, R. Tomasello, M. Carpentieri, and M. Klaui, Magnetic skyrmions: from fundamental to applications, *Journal of Physics D: Applied Physics*. **49**, 423001-(17) (2016).
- [42] W. Jiang, G. Chen, K. Liu, J. Zang, S. G. E. te Velthuis, and A. Hoffmann, Skyrmions in magnetic multilayers, *Physics Reports* **704**, 1-49 (2017).
- [43] A. Fert, N. Reyren, and V. Cros, Magnetic skyrmions: advances in physics and potential applications, *Nature Reviews Materials* **2**, 17031-(15) (2017). I
- [44] A. N. Bogdanov and D. A. Yablonskii, Thermodynamically stable "vortices" in magnetically ordered crystals. The mixed state of magnets. *Soviet Physics JETP* **68**, 101-103 (1989). I
- [45] A. Bogdanov and A. Hubert, Thermodynamically stable magnetic vortex states in magnetic crystals, *J. Magn. Mater.* **138**, 255-269 (1994). I
- [46] U. K. Röfler, N. Bogdanov, and C. Pfleiderer, Spontaneous skyrmion ground states in magnetic metals, *Nature* **442**, 797-801 (2006).
- [47] S. Heinze, K. von Bergmann, M. Menzel, J. Brede, A. Kubetzka, R. Wiesendanger, G. Bihlmayer, and S. Blugel, Spontaneous atomic-scale magnetic skyrmion lattice in two dimensions, *Nature Physics* **7**, 713-718 (2011).

- [48] O. Boulle, J. Vogel, H. Yang, S. Pizzini, D. de Souza Chaves, A. Locatelli, T. O. Mentes, A. Sala, L. D. Buda-Prejbeanu, O. Klein, M. Belmeguenai, Y. Roussigné, A. Stahkevich, S. M. Chérif, L. Aballe, M. Foerster, M. Chshiev, S. Auffret, I. M. Miron, and G. Gaudin, Room-temperature chiral magnetic skyrmions in ultrathin magnetic nanostructures, *Nature Nanotechnology* **11**, 449-454 (2016).
- [49] A. O. Leonov, T. L. Monchesky, N. Romming, A. Kubetzka, A. N. Bogdanov, and R. Wiesendanger, The properties of isolated chiral skyrmions in thin magnetic films, *New Journal of Physics* **18**, 065003-(16) (2016). I, II A
- [50] A. O. Leonov and M. Mostovoy, Multiply periodic states and isolated skyrmions in an anisotropic frustrated magnet, *Nature Communications* **6**, 8275-(8) (2015). I
- [51] X. Zhang, J. Xia, Y. Zhou, X. Liu, H. Zhang, and M. Ezawa, Skyrmion dynamics in a frustrated ferromagnetic film and current-induced helicity locking-unlocking transition, *Nature Communications* **8** 1717-(10) (2017). I
- [52] B. A. Ivanov, A. Y. Merkulov, V. A. Stepanovich, C. E. Zaspel, Finite energy solitons in highly anisotropic two dimensional ferromagnets, *Physical Review B* **74**, 224422-(17) (2006). I
- [53] S.-Z. Lin and S. Hayami, Ginzburg-Landau theory for skyrmions in inversion-symmetric magnets with competing interactions, *Physical Review B* **93**, 064430-(16) (2016). I
- [54] E. M. Chudnovsky and D. A. Garanin, Skyrmion glass in a 2D Heisenberg ferromagnet with quenched disorder, *New Journal of Physics* **20** 033006-(9) (2018). I
- [55] C. Moutafis, S. Komineas, and J. A. C. Bland, Dynamics and switching processes for magnetic bubbles in nanoelements, *Physical Review B* **79**, 224429-(8) (2009). I
- [56] X. Yu, Y. Onose, N. Kanazawa, J. Park, J. Han, Y. Matsui, N. Nagaosa, and Y. Tokura, Real-space observation of a two-dimensional skyrmion crystal, *Nature* **465**, 901-904 (2010). I
- [57] D. A. Garanin, E. M. Chudnovsky, S. Zhang, and X. X. Zhang, Thermal creation of skyrmions in ferromagnetic films with perpendicular anisotropy and Dzyaloshinskii-Moriya interaction, *Journal of Magnetism and Magnetic Materials* **493**, 165724-(9). I
- [58] T. Dohi, R. M. Reeve, and M. Kläui, Thin film skyrmionics, *Annual Review of Condensed Matter Physics* **33**, 73-95 (2022). I
- [59] D. Capic, D. A. Garanin, and E. M. Chudnovsky, Skyrmion-skyrmion interaction in a magnetic film, *Journal of Physics: Condensed Matter* **32**, 415803-(14) (2020). I, II A, II B
- [60] E. M. Chudnovsky and J. Tejada, *Lectures on Magnetism, Rinton Press, Princeton, New Jersey (2006)*. I
- [61] L. Cai, E. M. Chudnovsky, and D. A. Garanin, Collapse of skyrmions in two-dimensional ferromagnets and antiferromagnets, *Physical Review B* **86**, 024429-(4) (2012). II A
- [62] D. Capic, D. A. Garanin, and E. M. Chudnovsky, Stability of biskyrmions in centrosymmetric magnetic films, *Physical Review B* **100**, 014432 (2019). II A
- [63] R. E. Camley and K. L. Livedey, Consequences of Dzyaloshinskii-Motiya interaction, *Surface Science Reports* **78**, 100605-(33) (2023). II A
- [64] D. A. Garanin and E. M. Chudnovsky, Solid-liquid transition in a skyrmion matter, arXiv:2403.00151. I
- [65] A. Derras-Chouk, E. M. Chudnovsky, and D. A. Garanin, Quantum collapse of a magnetic skyrmion, *Physical Review B* **98**, 024423-(9) (2018).

II A